
Design of Static Passive Electromagnetic Skins (EMS) with Non-Radiating Currents

G. Oliveri, F. Zardi, P. Rocca, M. Salucci, and A. Massa

Contents

1	Introduction	3
2	Numerical Results	4
2.1	Square <i>EMS</i> ($P \times Q = 55 \times 55$), Diamond Forbidden Region, Trapezoid Footprint	4
2.1.1	Goal of the Analysis	4
2.1.2	Parameters	4
2.1.3	Results	6
2.1.4	Observations	19
2.2	Parametric Analysis over β , Square <i>EMS</i> ($P \times Q = 55 \times 55$), Diamond Forbidden Region	20
2.2.1	Goal of the Analysis	20
2.2.2	Parameters	20
2.2.3	Results	21
2.2.4	Observations	23

1 Introduction

This document discusses the research activity related to the design of static passive Electromagnetic Skins (*EMS*s) with forbidden regions, *i.e.*, regions where no Unit Cells (*UC*s) may be placed. To design such devices, the concept of Non-Radiating (*NR*) currents is exploited.

For the sake of clarity, Table I lists the acronyms used throughout this document.

Acronym	Meaning
<i>EMS</i>	Electro-Magnetic Skin
<i>FR</i>	Forbidden Region
<i>MN</i>	Minimum-Norm
<i>IPM</i>	Iterative Phase-Matching
<i>NR</i>	Non-Radiating
<i>SVD</i>	Singular Value Decomposition
<i>UC</i>	Unit Cell

Table I: List of acronyms.

2 Numerical Results

2.1 Square *EMS* ($P \times Q = 55 \times 55$), Diamond Forbidden Region, Trapezoid Footprint

2.1.1 Goal of the Analysis

The goal of the analysis is to demonstrate that, by exploiting the *NR* currents, it is possible to design a *EMS* with a diamond-shaped hole at its center.

2.1.2 Parameters

- *EMS* Geometry:
 - Frequency: $f = 3.5$ [GHz] ($\lambda \cong 8.57$ [cm]),
 - Number of elements: $P \times Q = 55 \times 55 = 3025$,
 - Unit Cell spacing along x and y : $\Delta_x = \Delta_y = 0.5\lambda \cong 4.29$ [cm],
 - Size along x and y : $L_x = L_y \cong 2.36$ [m],
 - Height from the ground: $H = 5$ [m].
- Incident Field: Plane Wave
 - Incidence Direction: normal incidence, $(\theta_i, \phi_i) = (0, 0)$ [deg]
 - Polarization: $E_{\theta,0}^i = 1$ [V/m], $E_{\phi,0}^i = 0$ [V/m]
- Forbidden Region: Diamond
 - Center: $(0, 0)$ [m]
 - Diagonal along x : $D_x = 0.55$ [m]
 - Diagonal along y : $D_y = 0.8$ [m]
- Target Pattern:
 - Shape: Trapezoid Footprint
 - * Horizontal distance between *EMS* and Trapezoid Center: 10 [m]
 - * Trapezoid minor basis: 2 [m]
 - * Trapezoid major basis: 3 [m]
 - * Trapezoid width: 4 [m]
 - Number of visible pattern samples: $M = 3207$
 - Upper mask, $\mathcal{U}(\mathbf{r})$:
 - * $\max\{\mathcal{U}(\mathbf{r})\} = 0$ [dB]

* $\min \{\mathcal{U}(\mathbf{r})\} = -60$ [dB]

– Lower mask, $\mathcal{L}(\mathbf{r})$:

* $\max \{\mathcal{L}(\mathbf{r})\} = -3$ [dB]

* $\min \{\mathcal{L}(\mathbf{r})\} = -120$ [dB]

- Truncated *SVD* threshold for *MN/NR* current decomposition: $T = 10^{-3}$
- Truncated *SVD* threshold for finding *NR* current coefficients: $\beta = 10^{-1}$

ELEDIA Research Center

2.1.3 Results

Target Pattern

The trapezoid lower and upper footprint masks are shown in Fig. 1(a) and Fig. 1(b), respectively.

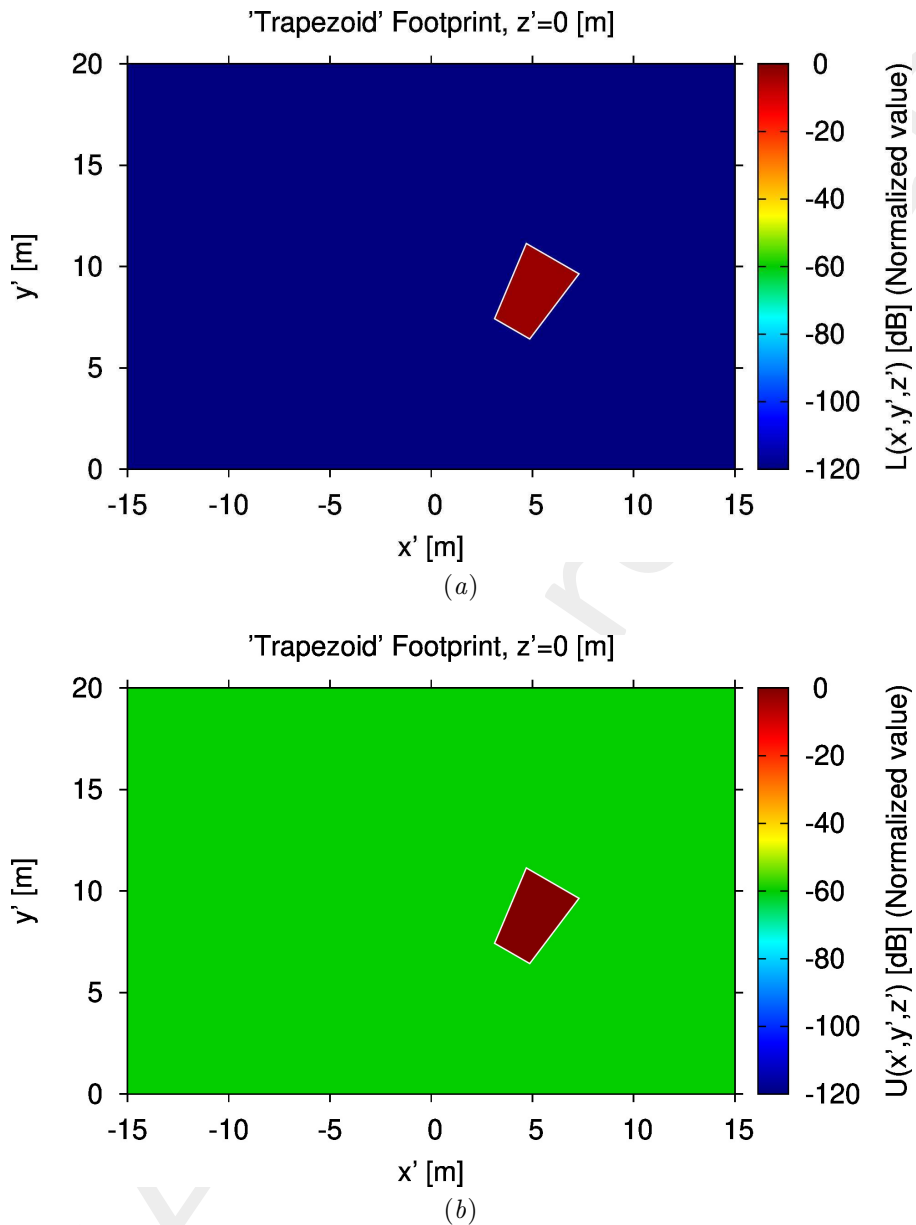


Figure 1: Masks used to obtain the footprint pattern with the *IPM*: (a) upper mask and (b) lower mask.

In order to have a feasible pattern as the target pattern, the *IPM* is applied to the footprint mask. The pattern radiated by the solution obtained with the *IPM* is then used as the target pattern in the subsequent analysis.

The magnitude and phase of the currents obtained with the *IPM* are shown in Fig. 2(a) and 2(b), respectively.

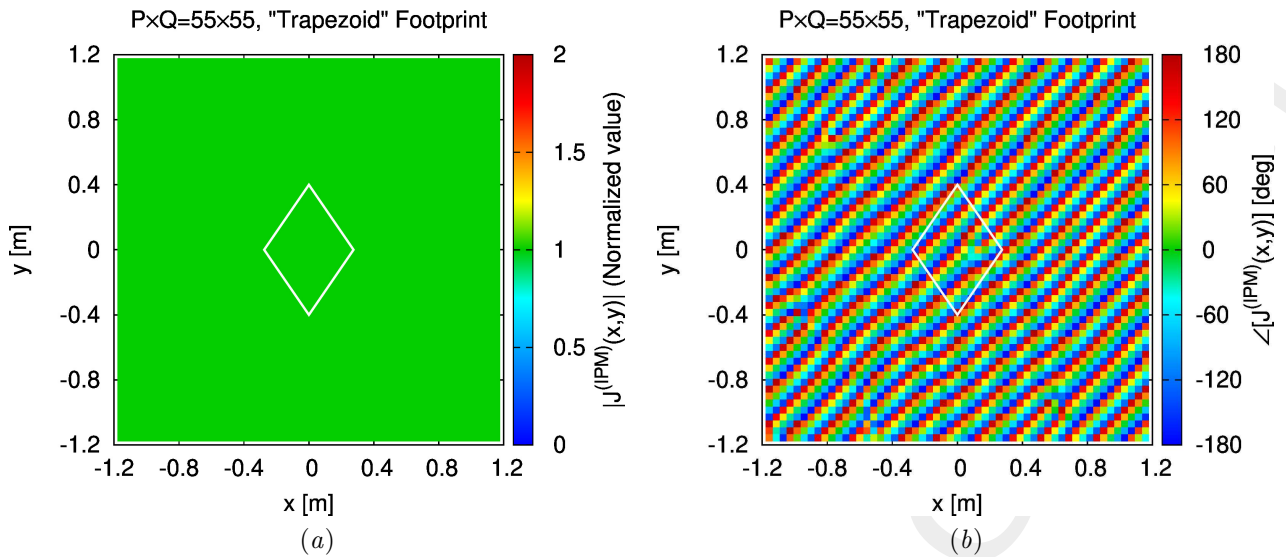


Figure 2: (a) Magnitude and (b) phase of the desired current distribution obtained with *IPM*.

The pattern radiated by the current distribution obtained with *IPM* is shown in Fig. 3.

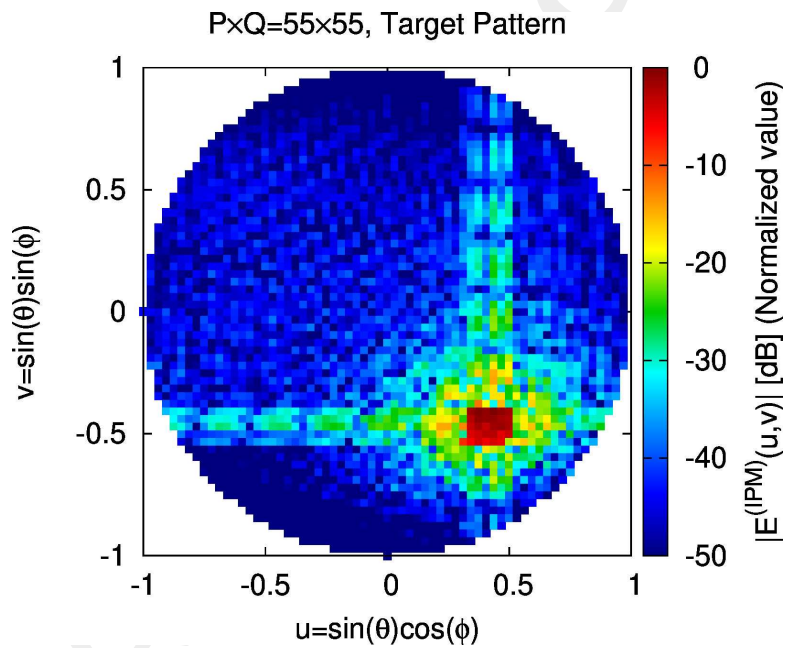


Figure 3: Pattern radiated by the current distribution found with *IPM*.

The footprint pattern radiated by the current distribution obtained with *IPM* is shown in Fig. 4, with a white line outlining the desired trapezoid footprint.

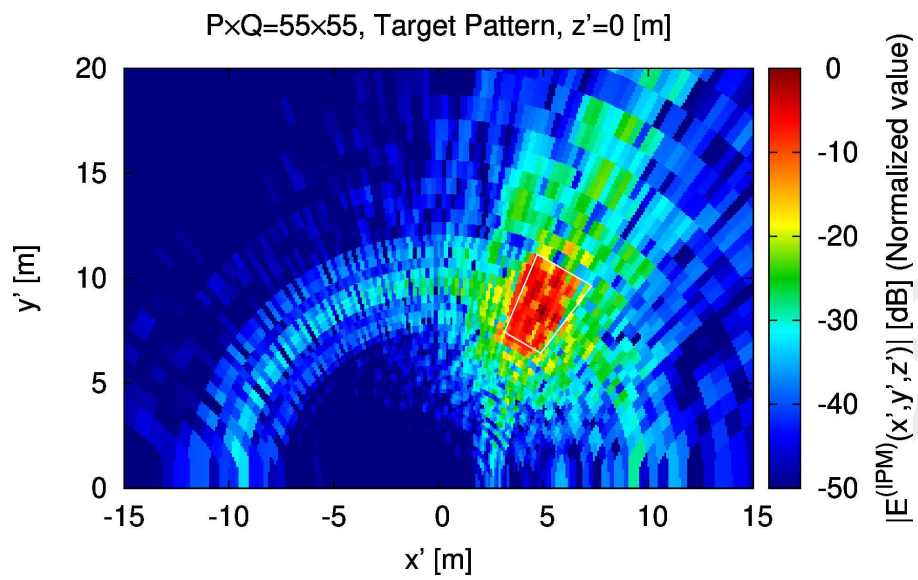


Figure 4: Footprint radiated by the current distribution found with *IPM*.

Target Current Synthesis: Standard Process

The green matrix is decomposed using SVD. The Singular Values of the Green matrix are shown in Fig. 5, along with the truncation threshold $T = 10^{-3}$.

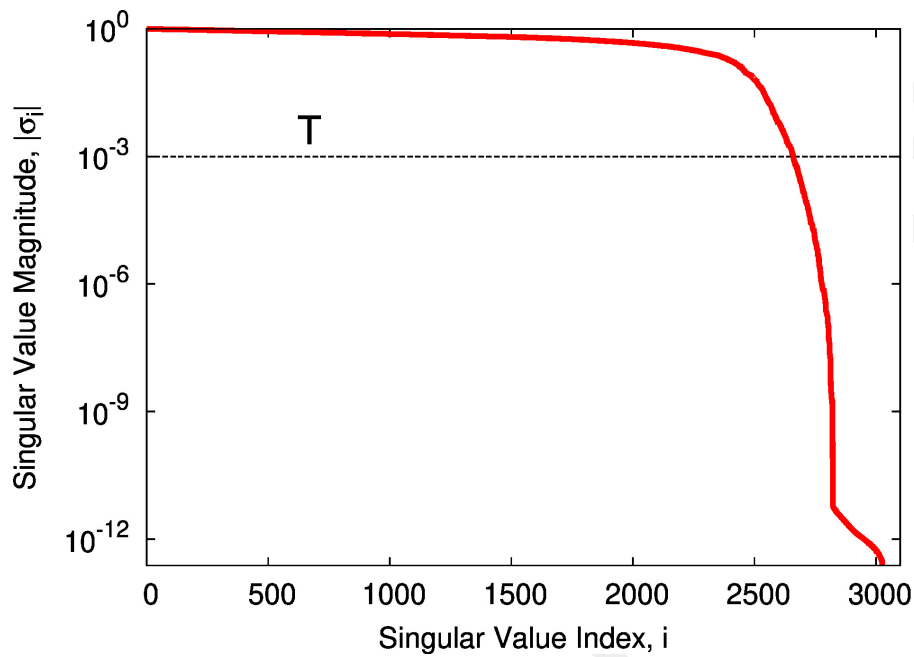


Figure 5: Singular Values of the Green Matrix.

The desired MN , NR , and total currents shown in Fig. 6 are obtained.

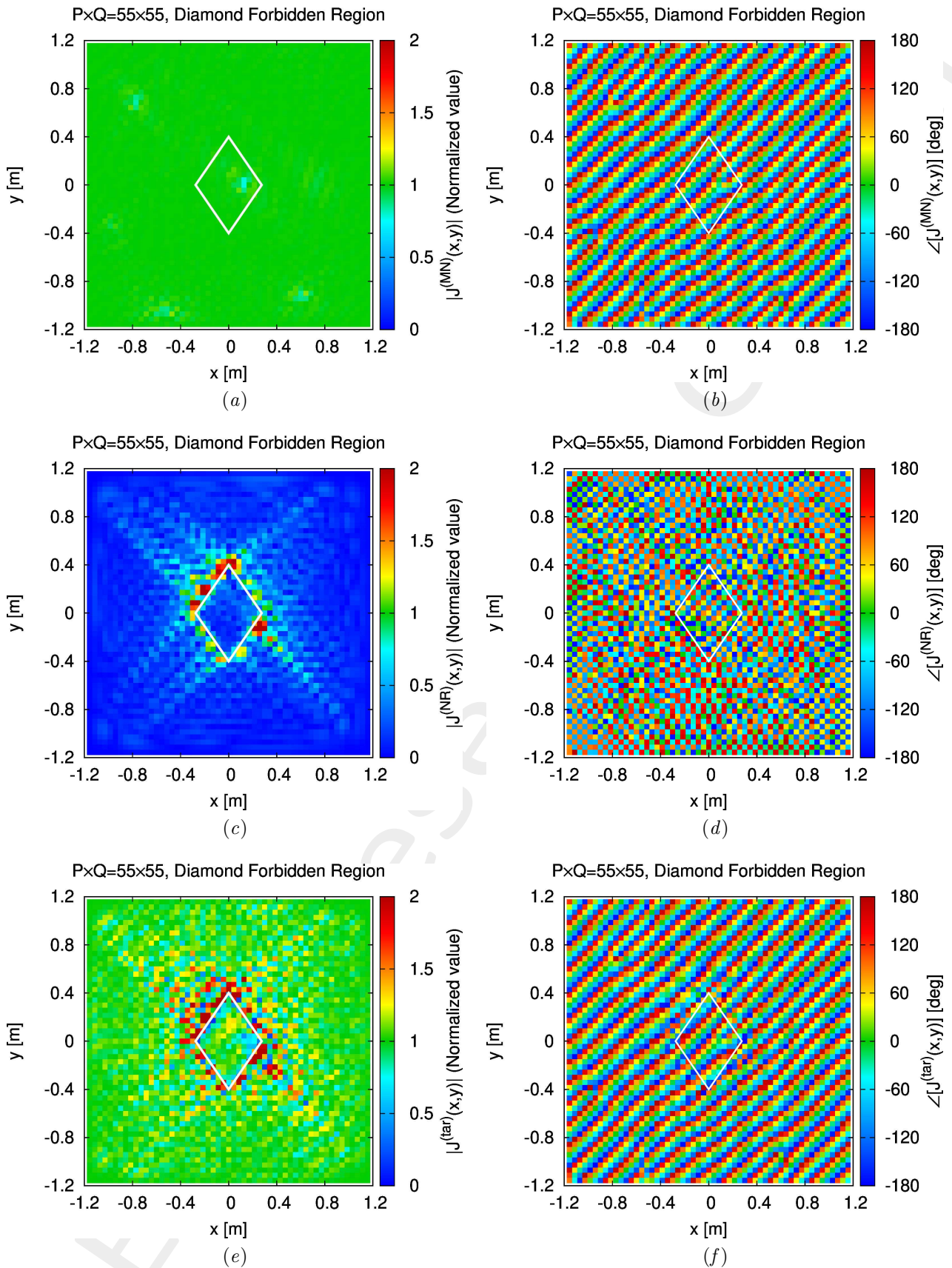


Figure 6: Current distributions obtained with the standard synthesis procedure: (a), (c), and (e) magnitude and (b), (d), and (f) phase of (a) and (b) Minimum-Norm component of the target current, (c) and (d) Non-Radiating component of the target current, and (e) and (f) total target current; .

Figure 7 shows the footprint pattern radiated by the MN , NR , and total currents previously shown in Fig. 6.

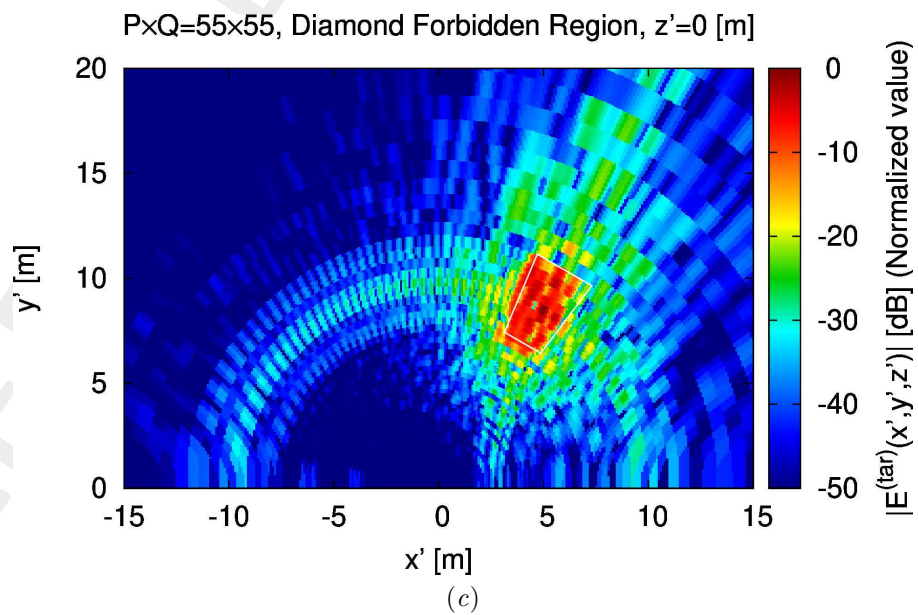
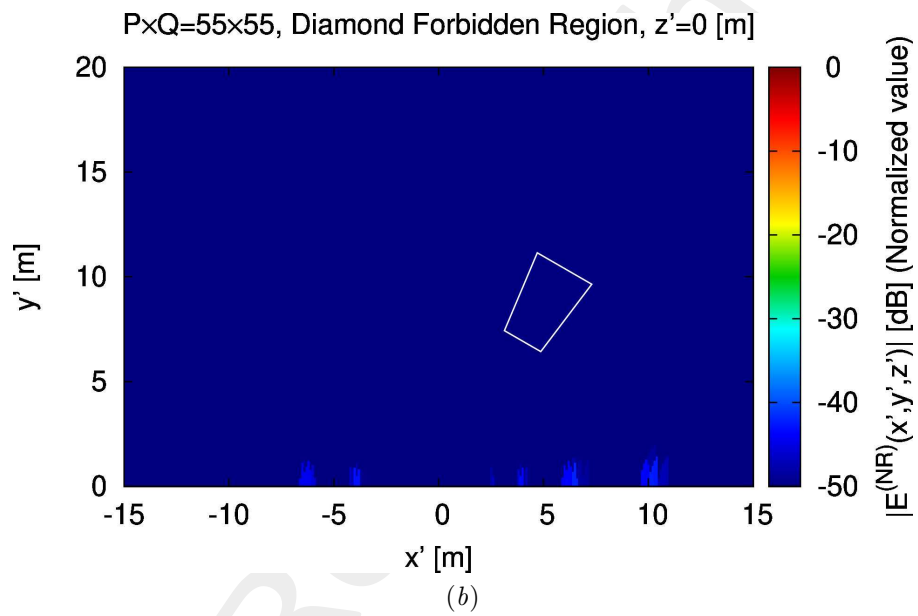
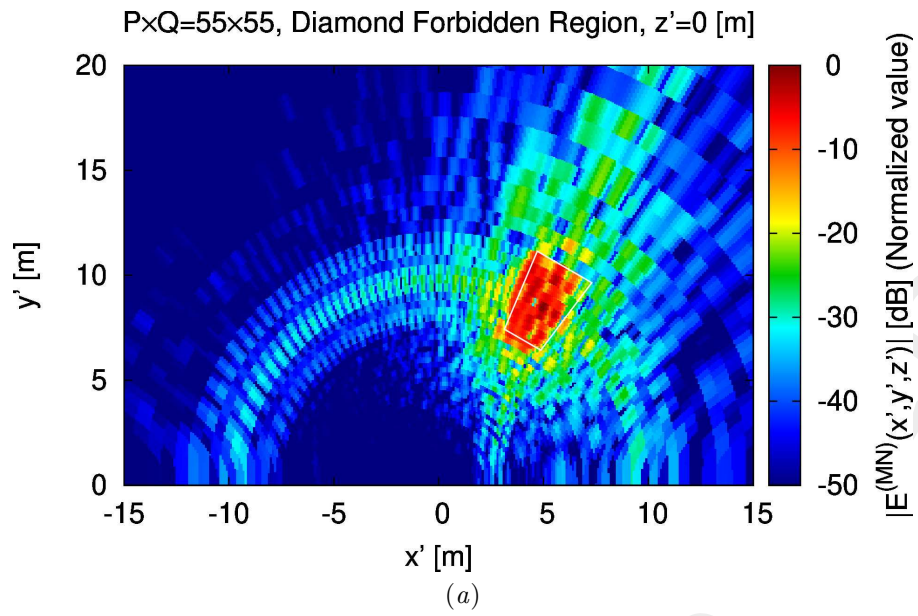


Figure 7: Footprint patterns radiated by different current distributions: (a) radiated by MN currents, (b) radiated by NR currents, and (c) radiated by the total currents.

Target Current Synthesis: Reverse Engineering

The target currents are recomputed from the synthesized Smart Skin with a reverse engineering process. The MN , NR , and total current distributions are shown in Fig. 8.

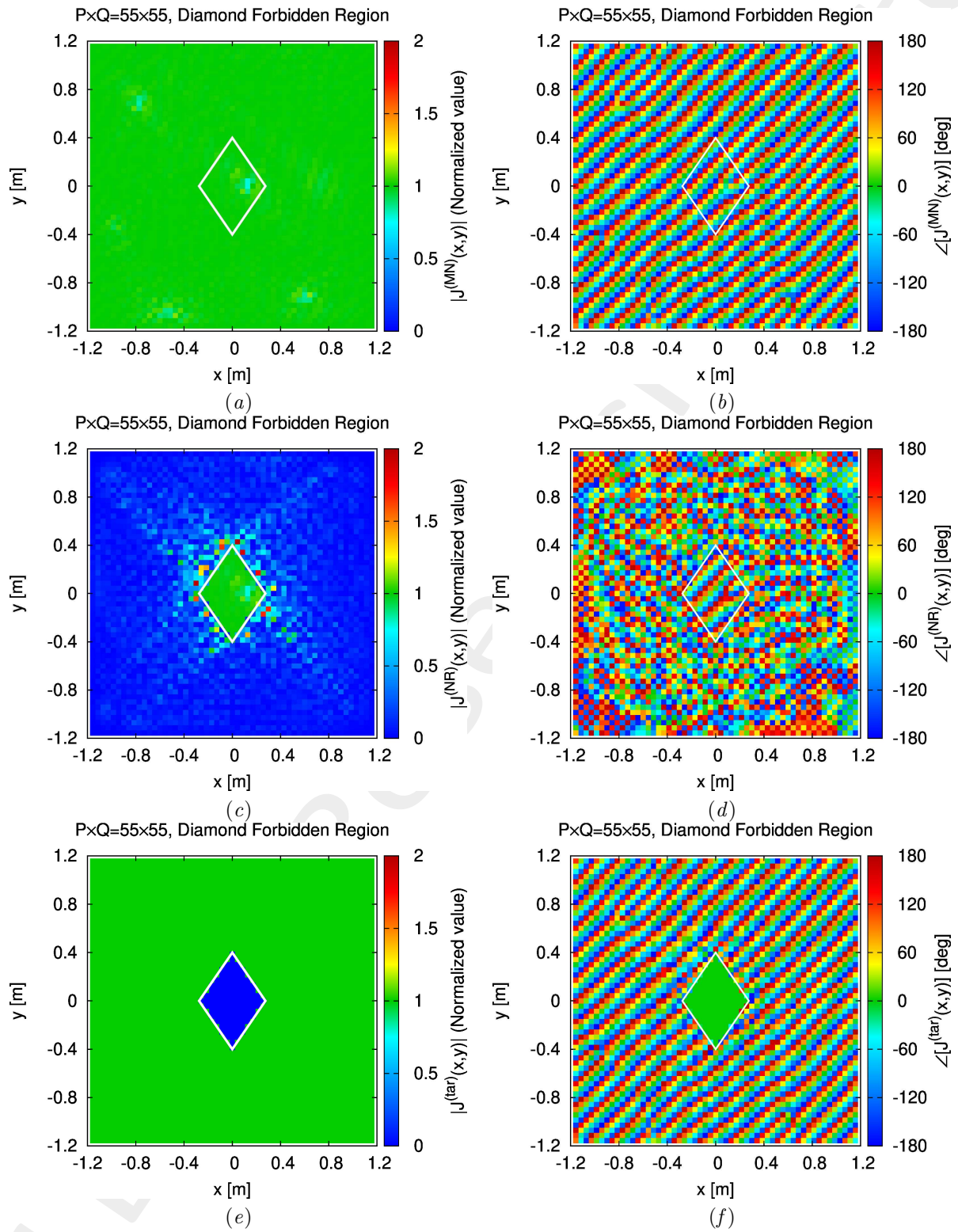


Figure 8: Current distributions obtained with reverse engineering: (a) and (b) MN component of the target current, (c) and (d) NR component of the target current, and (e) and (f) total target current; (a)(c)(e) magnitude and (b)(d)(f) phase.

Figure 9 shows the footprint pattern radiated by each current distribution of Fig. 8.

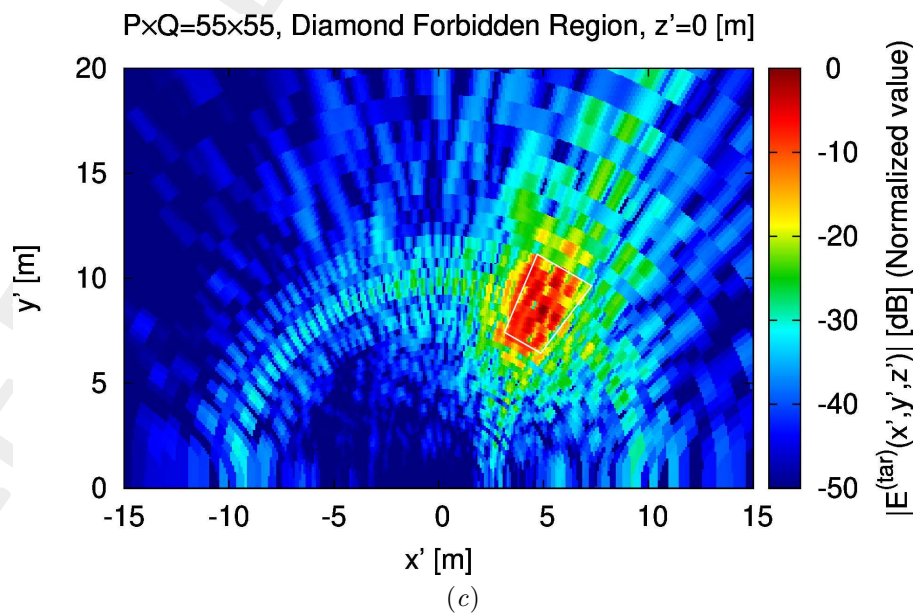
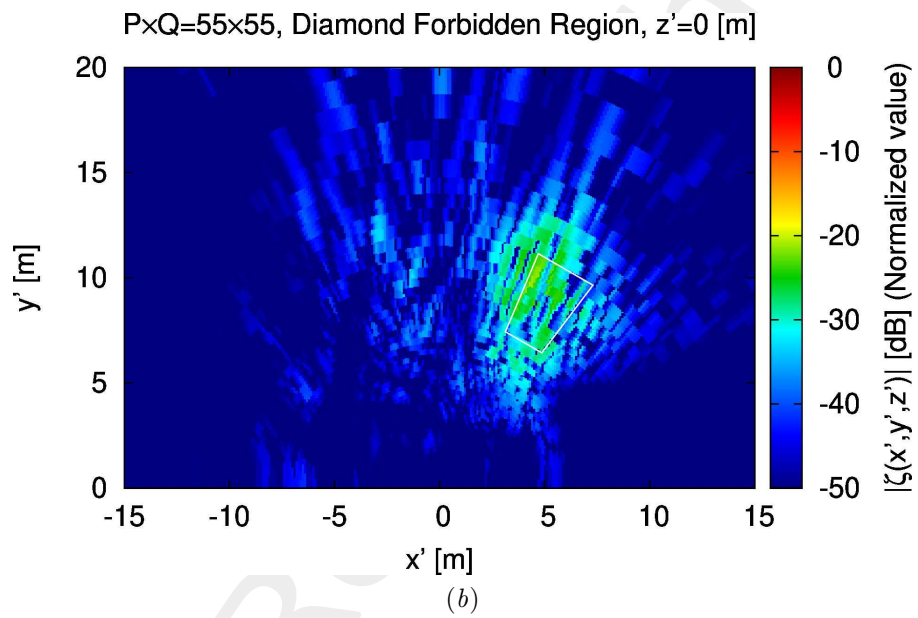
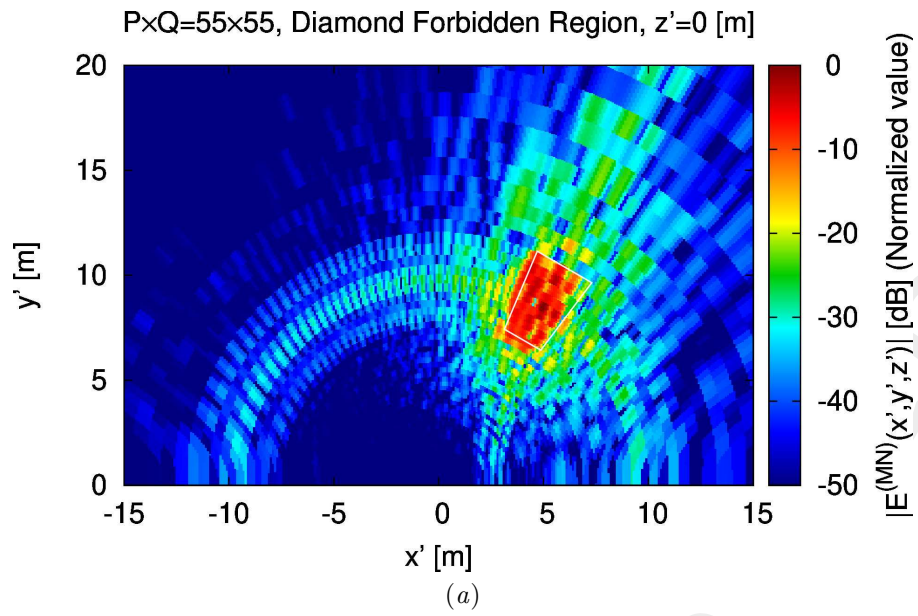


Figure 9: (a) Footprint pattern radiated by $J^{(MN)}$, (b) difference between footprints radiated by $J^{(tar)}$ and $J^{(MN)}$, and (c) footprint pattern radiated by $J^{(tar)}$.

EMS Design without Forbidden Region

An EMS is designed to reflect the target pattern *without* respecting the forbidden region. These results will be later used as a reference. Figure 10 shows the dimensions of the square patches on the designed EMS.

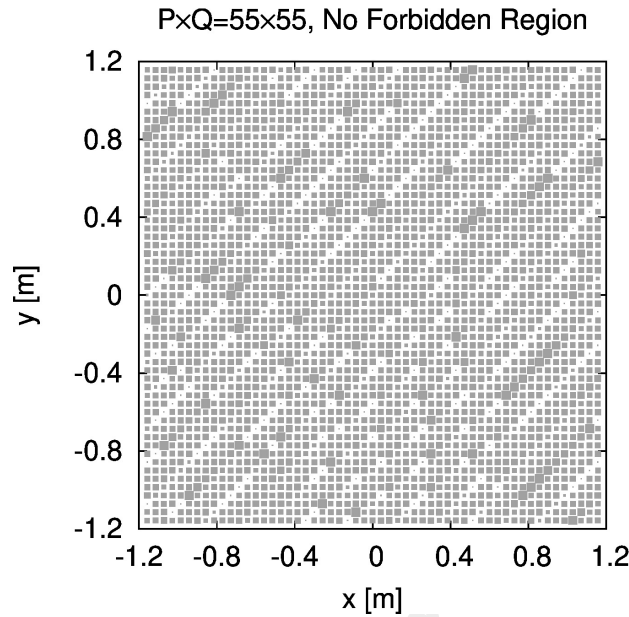


Figure 10: Dimensioning of the UCs on the EMS synthesized with no forbidden region.

The magnitude and phase of the magnetic current distribution equivalent to the EMS with forbidden region are shown in Fig. 11(a) and 11(b), respectively.

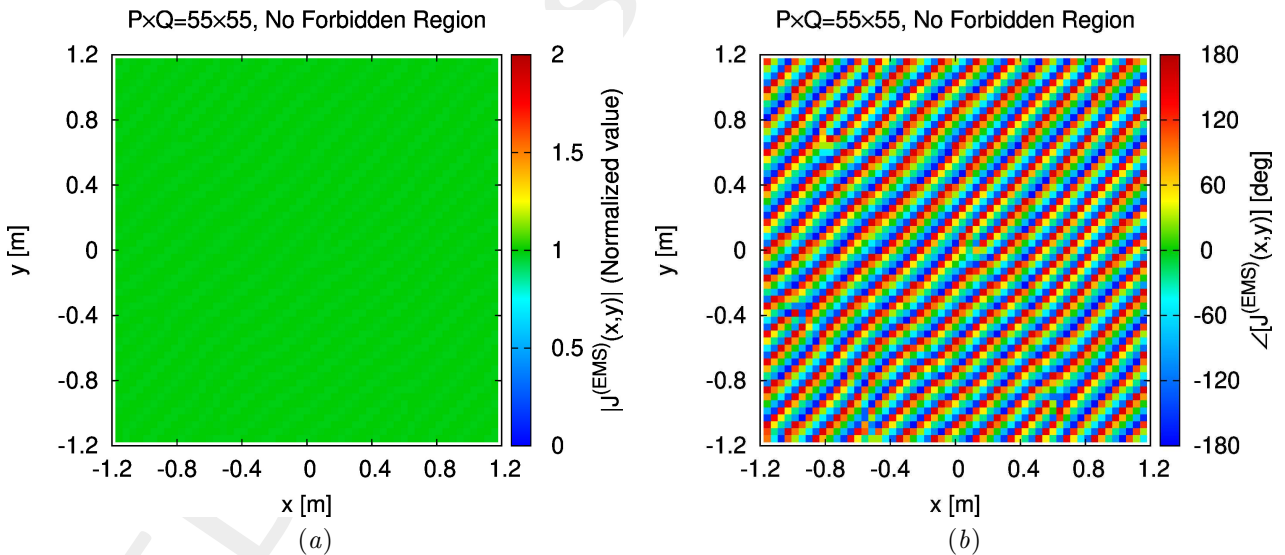


Figure 11: (a) Magnitude and (b) phase of the magnetic current equivalent to the EMS synthesized with no forbidden region.

Figure 12 shows the footprint pattern reflected by the EMS designed without forbidden region.

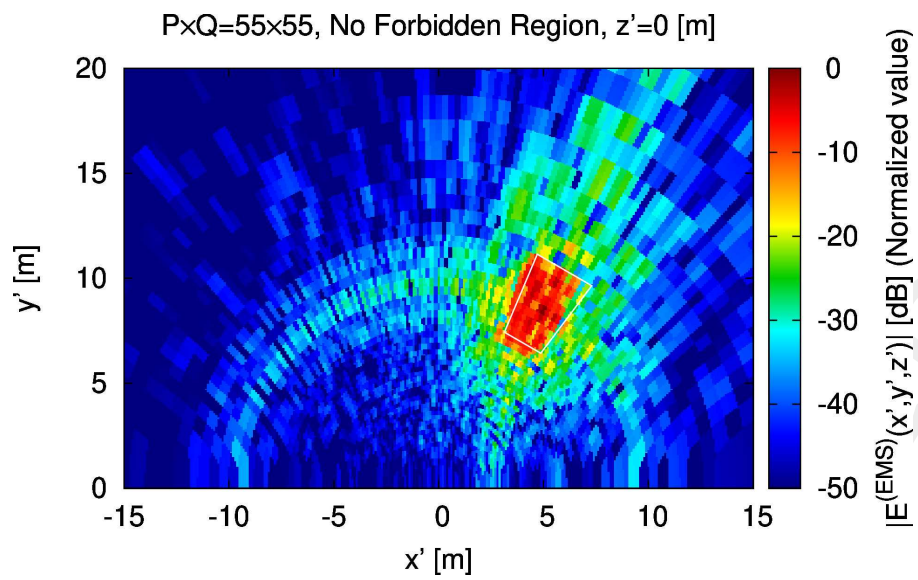


Figure 12: Footprint Pattern reflected by the *EMS* synthesized with no forbidden region.

ELEDIA Research Center

EMS Synthesis with Forbidden Region

A *EMS* is designed to synthesize the total target current, $J^{(tar)}$, with the diamond forbidden region. Figure 13 shows the dimensioning of the square patches on the designed *EMS*.

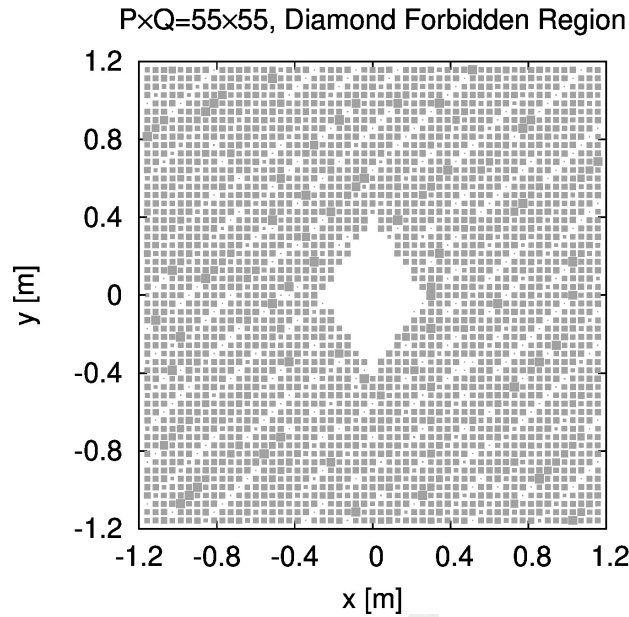


Figure 13: Dimensioning of the *UCs* of the *EMS* synthesized with a diamond forbidden region.

The magnitude and phase of the magnetic current distribution equivalent to the *EMS* with forbidden region are shown in Fig. 14(a) and 14(b), respectively.

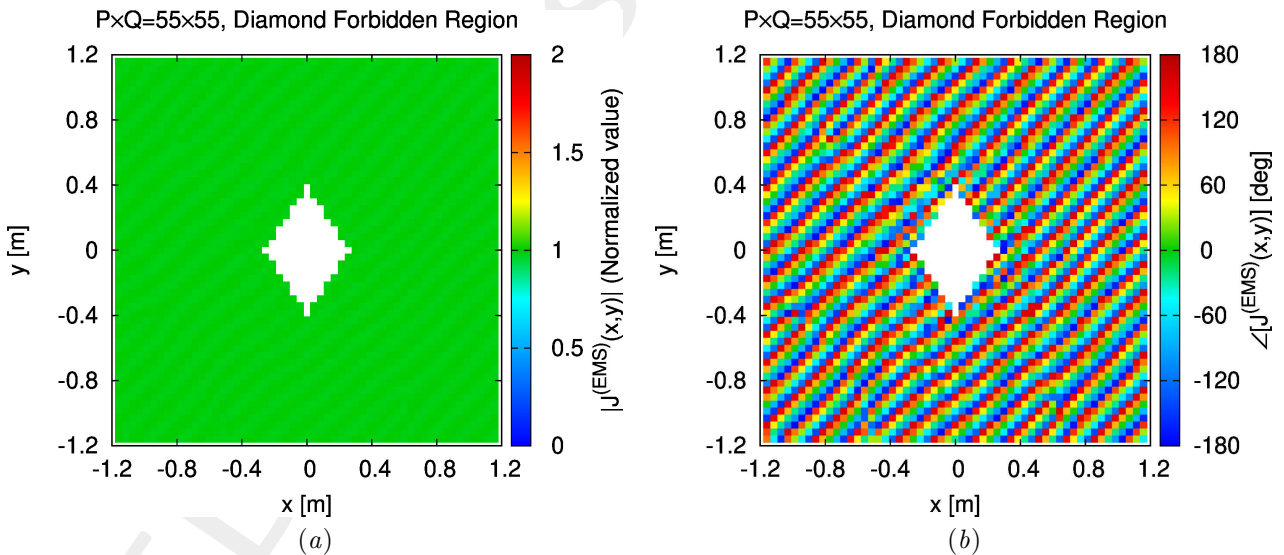


Figure 14: (a) Magnitude and (b) phase of the magnetic current equivalent to the *EMS* synthesized with diamond forbidden region.

Figure 15(a) shows the footprint pattern reflected by the *EMS* with the Forbidden Region, compared to the pattern radiated by the *EMS* without the Forbidden Region [Fig. 15(b)]. Additionally, the difference between the two footprint patterns is shown in Fig. 15(c).

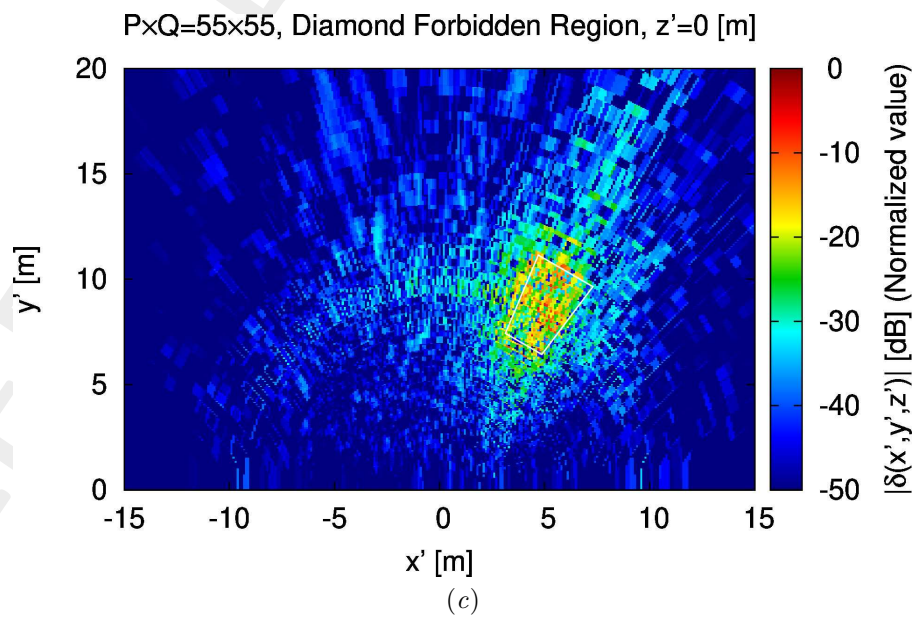
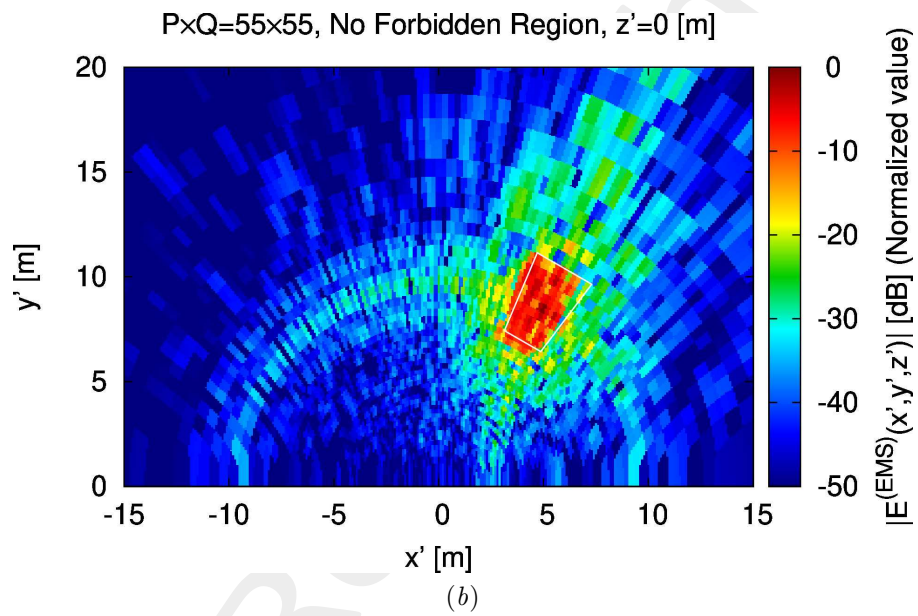
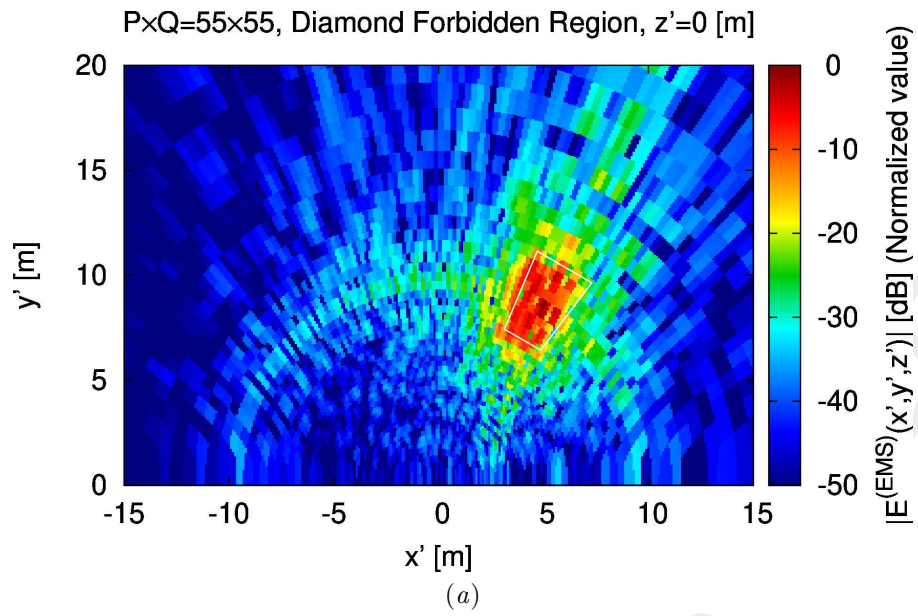


Figure 15: Footprint Pattern: (a) reflected by the *EMS* with a diamond forbidden region, (b) reflected by the *EMS* with no forbidden region, and (c) difference between the two patterns.

Finally, the mask violation is shown for the *EMS* with and without forbidden region in Fig. 16(a) and 16(b), respectively.

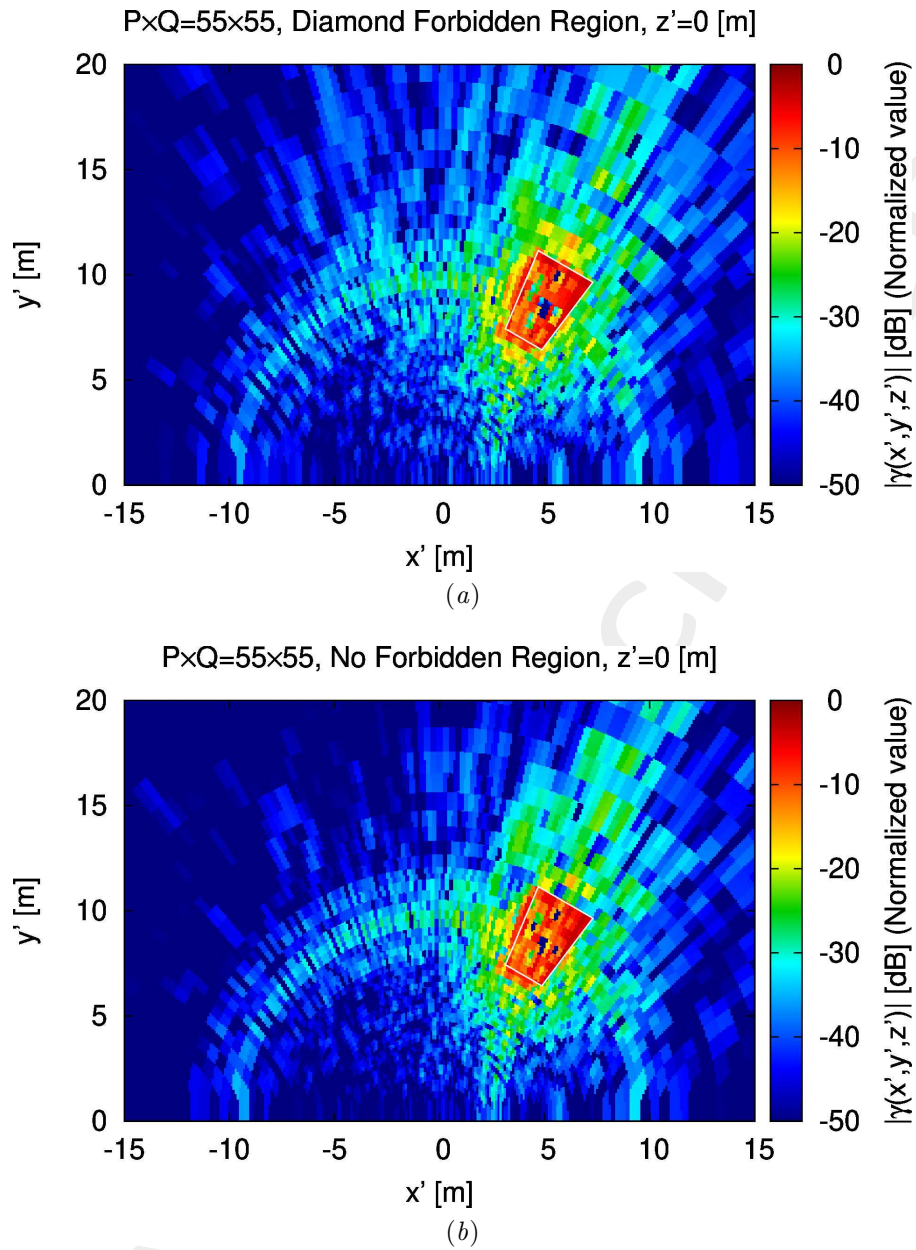


Figure 16: Mask violation for (a) the *EMS* with diamond forbidden region and (b) the *EMS* without forbidden region.

The average mask violation for the *EMS* with and without forbidden region are reported in Tab. II.

<i>EMS</i>	Average Mask Violation, $\gamma(\mathbf{r}')$	
	[linear]	[dB]
With Diamond Forbidden Region	0.153×10^{-1}	-36.28
Without Forbidden Region	0.136×10^{-1}	-37.28

Table II: Average mask violation for the *EMS* with and without forbidden region.

The computation times for the main tasks of the *EMS* synthesis process are summarized in Tab. III.

Task	Computation Time [sec]
Computation of Green matrix	7.66
<i>SVD</i> Decompositon	3.94×10^2
Computation of <i>NR</i> basis	2.50×10^1
Computation of <i>NR</i> coefficients	0.69×10^{-1}

Table III: Computation times for *EMS* synthesis.

2.1.4 Observations

- The design of a Smart Skin with a large, diamond forbidden region was successful;
- The currents obtained with the standard procedure, however, do not present $J^{(tar)} = 0$ in the forbidden region;
- The currents obtained with the reverse engineering present $J^{(tar)} = 0$ in the forbidden region, and the “*NR*” component have small impact on the footprint pattern.

2.2 Parametric Analysis over β , Square *EMS* ($P \times Q = 55 \times 55$), Diamond Forbidden Region

2.2.1 Goal of the Analysis

The goal of the analysis is to understand how the parameter β influences the outcomes of the *EMS* synthesis process.

2.2.2 Parameters

- *EMS* Geometry:
 - Frequency: $f = 3.5$ [GHz] ($\lambda \cong 8.57$ [cm]),
 - Number of elements: $P \times Q = 55 \times 55 = 3025$,
 - Unit Cell spacing along x and y : $\Delta_x = \Delta_y = 0.5\lambda \cong 4.29$ [cm],
 - Size along x and y : $L_x = L_y \cong 2.36$ [m],
 - Height from the ground: $H = 5$ [m].
- Incident Field: Plane Wave
 - Incidence Direction: normal incidence, $(\theta_i, \phi_i) = (0, 0)$ [deg]
 - Polarization: $E_{\theta,0}^i = 1$ [V/m], $E_{\phi,0}^i = 0$ [V/m]
- Forbidden Region: Diamond
 - Center: $(0, 0)$ [m]
 - Diagonal along x : $D_x = 0.55$ [m]
 - Diagonal along y : $D_y = 0.8$ [m]
- Target Pattern:
 - Shape: Trapezoid Footprint
 - * Horizontal distance between *EMS* and Trapezoid Center: 10 [m]
 - * Trapezoid minor basis: 2 [m]
 - * Trapezoid major basis: 3 [m]
 - * Trapezoid width: 4 [m]
 - Number of visible pattern samples: $M = 3207$
 - Upper mask, $\mathcal{U}(\mathbf{r})$:
 - * $\max \{\mathcal{U}(\mathbf{r})\} = 0$ [dB]
 - * $\min \{\mathcal{U}(\mathbf{r})\} = -60$ [dB]

– Lower mask, $\mathcal{L}(\mathbf{r})$:

* $\max \{\mathcal{L}(\mathbf{r})\} = -3$ [dB]

* $\min \{\mathcal{L}(\mathbf{r})\} = -120$ [dB]

- Truncated *SVD* threshold for MN/NR current decomposition: $T = 10^{-3}$
- Truncated *SVD* threshold for finding NR current coefficients: $\beta = 10^{-1}$
- Values of β being tested:

$$\beta \in \{10^{-1}, 10^{-2}, 10^{-3}, 10^{-4}, 0\} \quad (1)$$

2.2.3 Results

As described in the numerical results section, finding the coefficients of the NR currents, $\underline{c}^{(NR)}$, such that the total current is zero in the forbidden region means solving a linear system of equations

$$\underline{\underline{B}} \underline{c}^{(NR)} = -\underline{J}^{(MN)} \quad (2)$$

In practice, this can be achieved with the pseudo-inverse matrix. Computing such matrix requires setting a threshold β for the truncation of the singular values of the matrix $\underline{\underline{B}}$. Figure 17 shows the singular values of the matrix $\underline{\underline{B}}$.

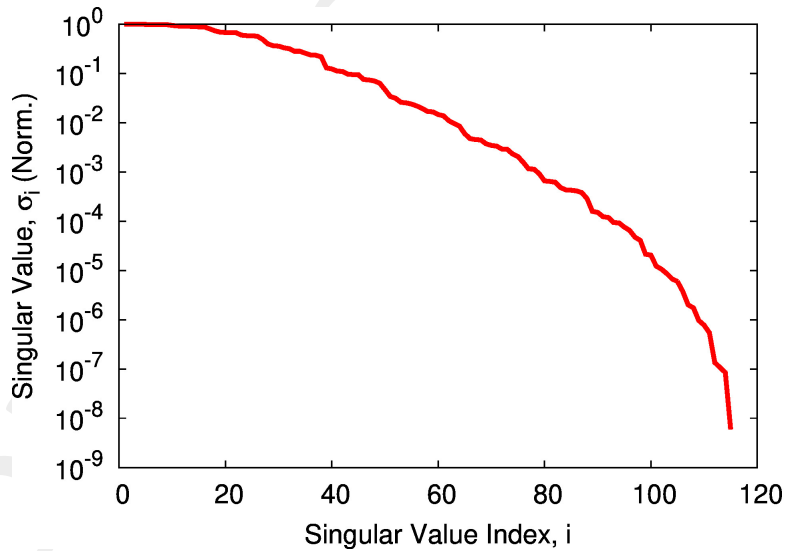


Figure 17: Singular values of the matrix $\underline{\underline{B}}$.

Figures 18 and 19 show, for different values of β , the magnitude of the total target current, $J^{(tar)}$, and the footprint reflected by the *EMS* designed to synthesize $J^{(tar)}$.

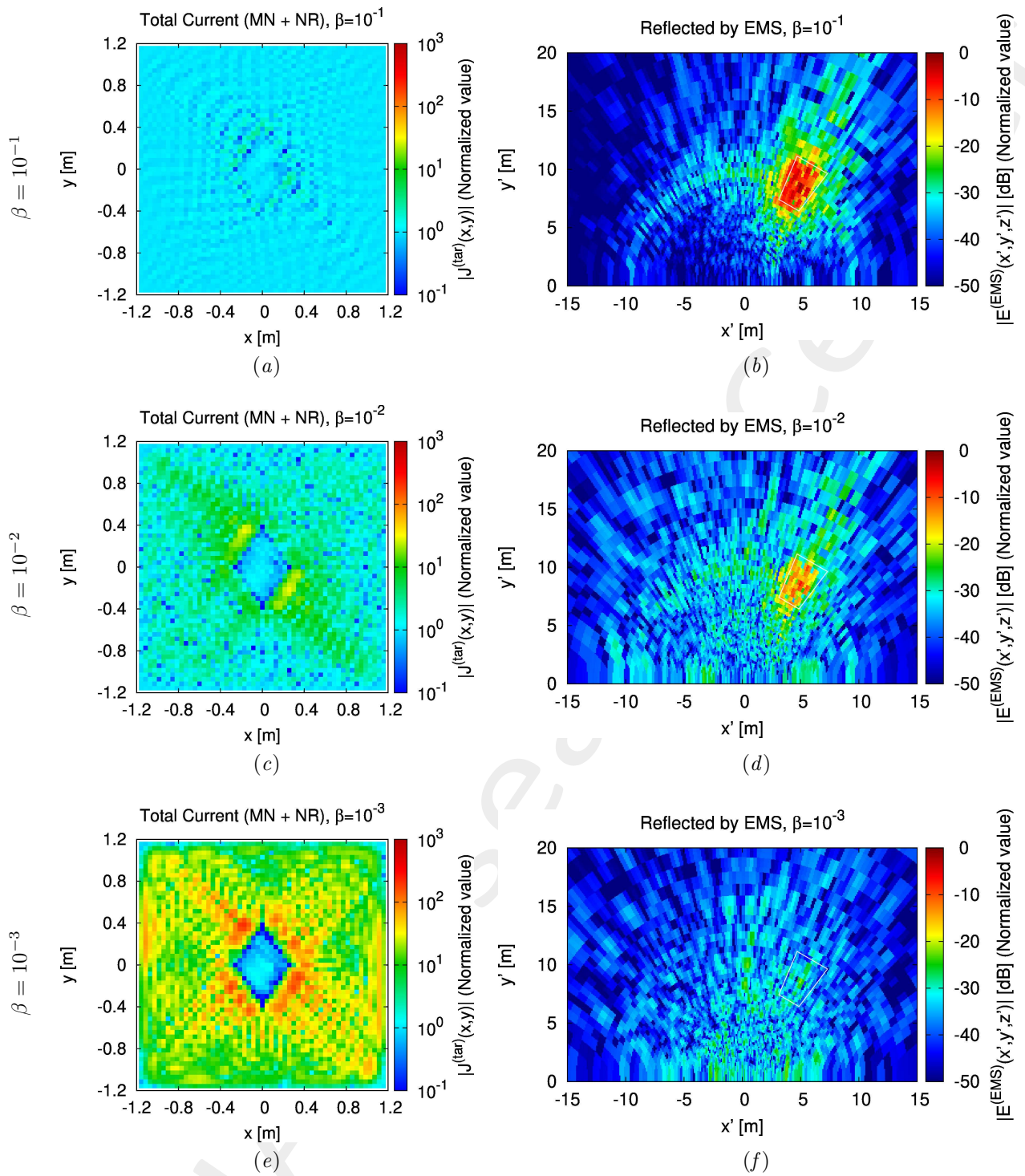


Figure 18: (a)(c)(e) Magnitude of the total target current, $J^{(tar)}$, and (b)(d)(f) footprint reflected by the resulting EMS for different values of β . (a)(b) $\beta = 10^{-1}$, (c)(d) $\beta = 10^{-2}$, and (e)(f) $\beta = 10^{-3}$.

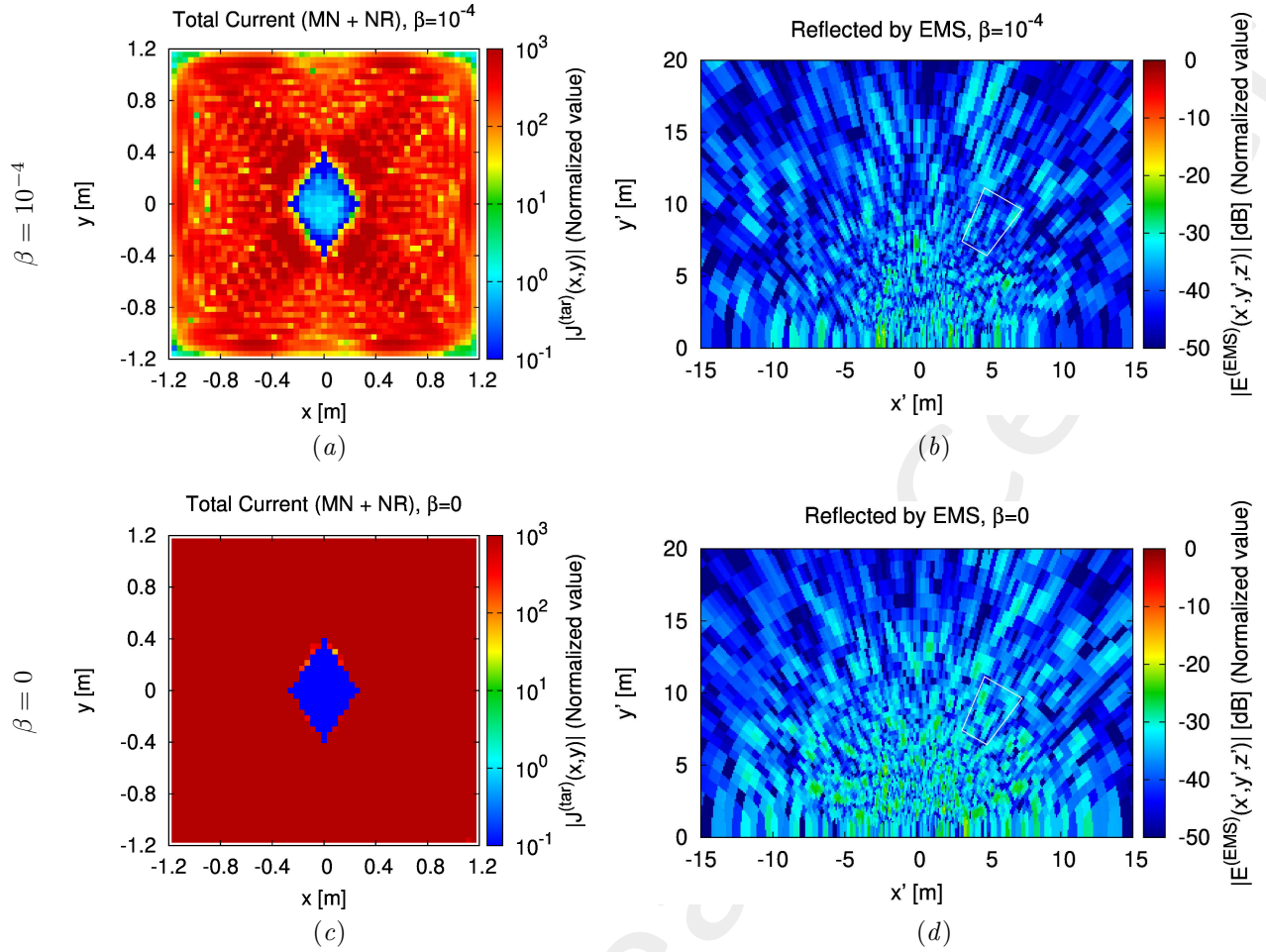


Figure 19: (a)(c) Magnitude of the total target current, $J^{(tar)}$, and (b)(d) footprint reflected by the resulting *EMS* for different values of β . (a)(b) $\beta = 10^{-4}$ and (c)(d) $\beta = 10^{-5}$.

2.2.4 Observations

The results indicate that,

- As the value of β decreases, the magnitude of $J^{(tar)}$ within the forbidden region decreases, until reaching zero for $\beta = 0$.
- As the value of β decreases, the magnitude of the $J^{(tar)}$ outside the forbidden region increases significantly, until reaching very large values ($J^{(tar)} > 10^3$ for $\beta = 0$).
- As the value of β decreases, the target current becomes impossible to synthesize with the *EMS*, and the footprint pattern is very far from the desired one.

More information on the topics of this document can be found in the following list of references.

References

- [1] A. Massa, A. Benoni, P. Da Ru, S. K. Goudos, B. Li, G. Oliveri, A. Polo, P. Rocca, and M. Salucci, "Designing smart electromagnetic environments for next-generation wireless communications," *Telecom*, Invited Paper, vol. 2, pp. 213-221, 2021.
- [2] A. Massa and G. Oliveri, "Metamaterial-by-Design: Theory, methods, and applications to communications and sensing - Editorial," *EPJ Applied Metamaterials*, vol. 3, no. E1, pp. 1-3, 2016.
- [3] G. Oliveri, D. H. Werner, and A. Massa, "Reconfigurable electromagnetics through metamaterials - A review" *Proc. IEEE*, vol. 103, no. 7, pp. 1034-1056, Jul. 2015.
- [4] M. Salucci, F. Boulos, A. Polo, and G. Oliveri, "Conformal transformation electromagnetics based on Schwarz-Christoffel mapping for the synthesis of doubly-connected metalenses," *IEEE Trans. Antennas Propag.*, vol. 68, no. 3, pp. 1836-1850, Mar. 2020.
- [5] M. Salucci, G. Oliveri, N. Anselmi, G. Gottardi, and A. Massa, "Performance enhancement of linear active electronically-scanned arrays by means of MbD-synthesized metalenses," *Journal of Electromagnetic Waves and Applications*, vol. 32, no. 8, pp. 927-955, 2018.
- [6] G. Oliveri, E. T. Bekele, M. Salucci, and A. Massa, "Transformation electromagnetics miniaturization of sectoral and conical horn antennas," *IEEE Trans. Antennas Propag.*, vol. 64, no. 4, pp. 1508-1513, April 2016.
- [7] G. Oliveri, E. T. Bekele, M. Salucci, and A. Massa, "Array miniaturization through QCTO-SI metamaterial radomes" *IEEE Trans. Antennas Propag.*, vol. 63, no. 8, pp. 3465-3476, Aug. 2015.
- [8] G. Oliveri, E. T. Bekele, D. H. Werner, J. P. Turpin, and A. Massa, "Generalized QCTO for metamaterial-lens-coated conformal arrays," *IEEE Trans. Antennas Propag.*, vol. 62, no. 8, pp 4089-4095, Aug. 2014.
- [9] G. Oliveri, L. Tenuti, E. Bekele, M. Carlin, and A. Massa, "An SbD-QCTO approach to the synthesis of isotropic metamaterial lenses," *IEEE Antennas Wirel. Propag. Lett.*, vol. 13, pp. 1783-1786, 2014.
- [10] M. Salucci, L. Tenuti, G. Gottardi, A. Hannan, and A. Massa, "System-by-design method for efficient linear array miniaturisation through low-complexity isotropic lenses" *Electronic Letters*, vol. 55, no. 8, pp. 433-434, May 2019.
- [11] M. Salucci, G. Oliveri, N. Anselmi, and A. Massa, "Material-by-design synthesis of conformal miniaturized linear phased arrays," *IEEE Access*, vol. 6, pp. 26367-26382, 2018.
- [12] G. Oliveri, M. Salucci, N. Anselmi, and A. Massa, "Multiscale System-by-Design synthesis of printed WAIMs for waveguide array enhancement," *IEEE J. Multiscale Multiphysics Computat. Techn.*, vol. 2, pp. 84-96, 2017.

-
- [13] G. Oliveri, F. Viani, N. Anselmi, and A. Massa, "Synthesis of multi-layer WAIM coatings for planar phased arrays within the system-by-design framework," *IEEE Trans. Antennas Propag.*, vol. 63, no. 6, pp. 2482-2496, June 2015.
- [14] G. Oliveri, M. Salucci, and A. Massa, "Generalized analysis and unified design of EM skins," *IEEE Trans Antennas Propag.*, vol. 71, no. 8, pp. 6579-6592, August 2023 (DOI: 10.1109/TAP.2023.3281073).
- [15] M. Salucci and A. Massa, "Unconventional sources for smart EM environments: An inverse scattering vision," *Reviews of Electromagnetics*, Invited Paper, vol 1, pp. 17-18, 2022 (DOI: 10.53792/roe/2022.1/21012).
- [16] M. Salucci, A. Benoni, G. Oliveri, P. Rocca, B. Li, and A. Massa, "A multihop strategy for the planning of EM skins in a smart electromagnetic environment," *IEEE Trans Antennas Propag.*, vol. 71, no. 3, pp. 2758-2767, March 2023 (DOI: 10.1109/TAP.2022.3233714).
- [17] G. Oliveri, F. Zardi, P. Rocca, M. Salucci, and A. Massa, "Constrained-design of passive static EM skins," *IEEE Trans. Antennas Propag.*, vol. 71, no. 2, pp. 1528-1538, February 2023 (DOI: 10.1109/TAP.2022.3225593).
- [18] G. Oliveri, P. Rocca, M. Salucci, D. Erricolo, and A. Massa, "Multi-scale single-bit RP-EMS synthesis for advanced propagation manipulation through system-by-design," *IEEE Trans. Antennas Propag.*, vol. 70, no. 10, pp. 8809-8824, October 2022 (DOI: 10.1109/TAP.2022.3201700).
- [19] A. Benoni, M. Salucci, G. Oliveri, P. Rocca, B. Li, and A. Massa, "Planning of EM skins for improved quality-of-service in urban areas," *IEEE Trans. Antennas Propag. - Special Issue on 'Smart Electromagnetic Environment,'* vol. 70, no. 10, pp. 8849-8862, October 2022 (DOI: 10.1109/TAP.2022.3177284).
- [20] G. Oliveri, F. Zardi, P. Rocca, M. Salucci, and A. Massa, "Building a smart EM environment - AI-Enhanced aperiodic micro-scale design of passive EM skins," *IEEE Trans. Antennas Propag. - Special Issue on 'Smart Electromagnetic Environment,'* vol. 70, no. 10, pp. 8757-8770, October 2022.
- [21] P. Rocca, P. Da Ru, N. Anselmi, M. Salucci, G. Oliveri, D. Erricolo, and A. Massa, "On the design of modular reflecting EM skins for enhanced urban wireless coverage," *IEEE Trans. Antennas Propag. - Special Issue on 'Smart Electromagnetic Environment,'* vol. 70, no. 10, pp. 8771-8784, October 2022.
- [22] G. Oliveri, P. Rocca, M. Salucci, and A. Massa, "Holographic smart EM skins for advanced beam power shaping in next generation wireless environments," *IEEE J. Multiscale Multiphys. Comput. Tech.*, vol. 6, pp. 171-182, Oct. 2021.